Effects of Torso-Borne Mass and Loading Severity on Early Response of the Lumbar Spine under High-Rate Vertical Loading

JiangYue Zhang*, Andrew C. Merkle, Catherine M. Carneal, Robert S. Armiger,
Reuben H. Kraft, Emily E. Ward, Kyle A. Ott, Alexis C. Wickwire,
Christopher J. Dooley, Timothy P. Harrigan, Jack C. Roberts

The Johns Hopkins University Applied Physics Laboratory

Abstract

Severities and types of under-body blast lumbar injuries maybe associated with loading severity and amount of torso-borne mass, such as personal protective equipment. The objective of this study was to delineate these effects using a high-fidelity pelvis-lumbar spine finite element model (FEM).

Geometries of the FEM was reconstructed from computed tomography scans and scaled to 50th percentile male. Hexagonal solid elements were used for majority of the FEM, except shell elements for cortical shells and endplates and nonlinear springs for ligaments. Material properties were obtained from in-house high-rate bulk and shear testing when available. Pelvis acceleration loadings were obtained from full-body Hybrid-III FEM. Simulations were conducted with high and low pelvis accelerations, with and without torso-borne mass. Results found loading modes in the spine progressively changes from flexion, to compression, and extension from upper to mid- and lower level resulted in an "S" shaped deformation, indicating change of injury mechanisms along the spine. Localized spine deformation decoupled the torso-borne mass from the high-rate pelvis acceleration during the initial stage (20-30ms). Under high pelvis acceleration, the spine may fail before the torso mass is engaged. Under low severity and lateral stage, motion of torso mass needs to be considered.

Keywords: Finite element model; Loading Severity; Lumbar spine injury; Torso-borne mass; Under-body blast.

I. INTRODUCTION

Improvised explosive devices (IED) have been a major threat to ground vehicles in the conflicts in Iraq and Afghanistan [1, 2]. During underbody blast (UBB) events, the vehicle structure is exposed to extreme blast forces at very high loading rates. The blast impulse is transferred from the structure through the floor and seat to the occupant, resulting in force transfer, blunt trauma and accelerative injuries. Studies have shown that the spine, specifically the thoracolumbar region, sustains significant injuries during UBB incidents [3-5]. The transfer of energy from the seat to the pelvis and subsequently to the spine has been considered the major injury mechanism for lumbar spine injury [3-6]. The patterns of these injuries suggest multiple potential loading mechanisms including dominant compressive loading (wedge fractures and burst fractures) and flexion-distraction injuries (Chance fractures).

To quantify blast loading to the vehicle and occupant, live fire blast tests have been conducted recently using a generic V-hull and Hybrid-III dummy [7]. Seat and floor accelerations and Hybrid-III responses have been commonly reported in these studies. However, it is generally agreed the Hybrid-III dummy was originally developed for blunt impact test in the horizontal plane. Its biofidelity in the vertical loading direction has never been validated. Therefore, Hybrid-III dummy response from these tests is not adequate for occupant injury assessment and injury mechanism analysis.

A project was initiated by the Johns Hopkins University Applied Physics Laboratory (JHU APL) to develop biomedically validated human Computational Models for Blast Injury Prevention (CoMBIP). The intent is to develop human models capable of simulating and predicting blast-induced injury, validated by biomechanical testing and being exercised under relevant loading conditions. An initial focus of CoMBIP was the development of a pelvis and spine for blast load investigation.

*JiangYue Zhang is Sr. Professional Staff in Research & Exploratory Development Department at The Johns Hopkins University - Applied Physics Laboratory in Laurel, MD 21042, USA (240-228-4540, 240-228-5889 (Fax), JiangYue.Zhang@jhuapl.edu).

Computational models of the pelvis and lumbar spine can be used to better understand the relationship between vertical seat acceleration and induced pelvis and lumbar injuries. The model can use actual seat acceleration measurements from live fire tests and apply it as the input to the pelvis to simulate the biomechanical response of the system. Analysis of the biomechanical response will not only help to understand the mechanisms of injury, but also help to establish boundary and loading conditions for high-rate PMHS material property testing and lumbar spine sub-system dynamic response testing.

Historically, lumbar spine finite element models (FEMs) have been constructed to study chronic degenerative diseases and surgical instrumentation under quasi-static loading [8-12] and therefore employed quasi-static material properties. The predominantly vertical loading direction in UBB events requires that FEM validation studies using biological tissue testing be performed accordingly; a number of dynamic FEMs have been validated in horizontal loading for vehicle crash injury studies [13, 14].

In addition, spine and pelvis postures are believed to have significant impact on biomechanical response of the pelvis & spine during UBB loading. It is essential to properly initialize the model to a correct sitting posture in order to properly simulate UBB injuries to occupants in a vehicle. Increase in loading severity and additional torso-borne mass are generally believed to increase lumbar spine loading during UBB events. However, the effects of these factors, including the relationships they may have with various injury mechanisms, have not been fully investigated and quantified.

The purpose of this study is to use a finite element model of the lumbar spine to assess injury mechanism in vertical loading, and to assess the effect of posture and torso-borne mass on these injury mechanisms.

II. METHODS

For this purpose, an integrated lumbar spine/pelvis/femur model was specifically developed at JHU APL for vertical acceleration along the lumbar spine. The model was properly positioned into sitting posture at every spine level, pelvis and femur and then used to simulate lumbar spine responses under two levels of UBB loading severities with and without torso borne-mass to study the effects of these factors.

Lumbar Spine/Pelvis/Femur Finite Element Model Development

A human lumbar spine FEM was previously developed at JHU/APL [15]. The source geometry of the model was based on the lumbar spine geometry from the male subject in the Visible Human Project [16-18]. Based on the anthropometric dimension of US adults (PEOPLESIZE program http://www.openerg.com/psz/index.htm), the visible human anatomies were transformed to match body measurements and organ volume of a 50^{th} percentile male. Detailed scaling method can be found in literature [17]. In addition, a forced left/right symmetry was performed by average the original with its mid-sagittal mirror [15]. These two generalization procedures created 50^{th} percentile male that is representative of larger populations.

A parametric, eight node hexahedral finite element mesh was developed based on the generalized geometry using TrueGrid software (XYZ Scientific Applications, Inc. Livermore, CA USA). The lumbar spine model consisted of all essential load bearing spine components from the T12/L1 intervertebral disc to the L5/S1 intervertebral disc. High-rate material properties of the lumbar spine intervertebral disc annulus and nucleus were obtained from split Hopkinson bar bulk and shear experiments [15, 19-21]. The automatic penalty driven slave/master contact method in LS-DYNA was used to simulate the facet joints from L1/L2 to L5/S1 in the lumbar spine. The ligaments were simulated as nonlinear springs in the current model. Material properties used for spine components were shown in

Table 1. Validations of the model have been conducted under quasi-static axial compression. A linearly increasing axial compression load of 700N was applied to the top of L1 while the bottom of L5 vertebrae was fixed in space. Axial displacement of each vertebral body was compared to reported literature data (Fig. 1) [22].

In this study, pelvis and femur FEMs have been recently developed following a similar procedure. The integrated pelvis-femur model consisted of the sacrum, left/right ilium, and left/right femur. Rigid links were used to simulate the sacroiliac joints and pubic symphysis (Fig. 2a). Spherical ball joints were used to simulate the femoroacetabular joint (Fig. 2b). Integration between the pelvis model and the lumbar spine model was completed using a rigid link between the superior surface of the sacrum and the inferior surface of the L5/S1

intervertebral disc, and surface to surface contact between the L5/Sacrum facet joints (Fig. 2c). The rigid link and the contact definitions coupled the pelvis kinematics to the lumbar spine model, creating an integrated lumbar spine/pelvis/femur model as shown in Fig. **2**d.

Table 1 Material properties of the model

Tissue	E (MPa)	ν	Reference
Cortical bone	12,000	0.3	Kuo, 2010
Cancellous bone	100	0.2	Shaw, 2007
Endplate	25	0.3	Guan, 2006
Posterior elements	3,500	0.25	Shirazi, 1986
Nucleus	K=3800	Elastic Fluid	
Annulus	4.5	0.3	

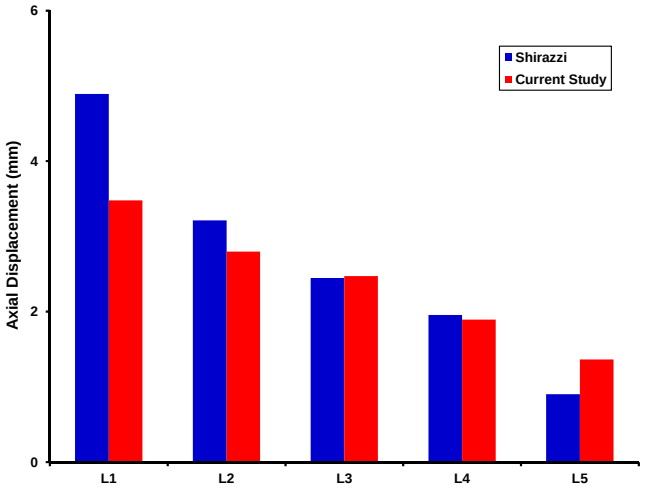

Fig. 1 Comparison of axial displacement of each lumbar spine segmental to literature data[22].

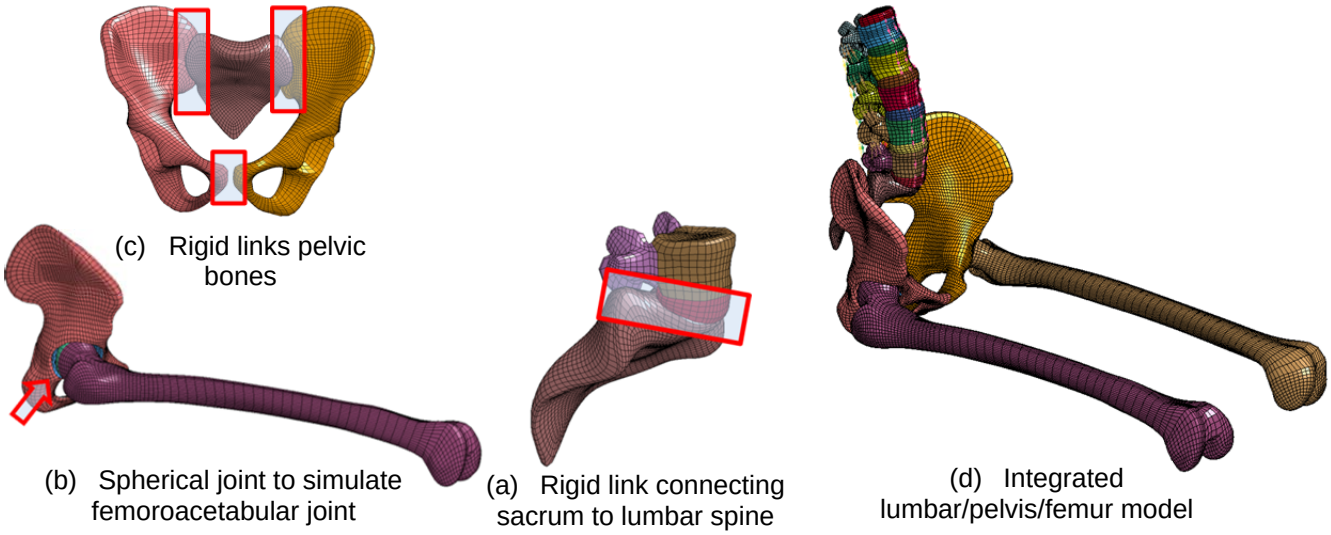

Fig. 2 Integration of lumbar/pelvis/femur FEM.

Reposition Model for 90/90/90 Sitting Posture

Since the influence of posture on biomechanical response for UBB loading is considered an important contributing factor to injury risk, it is essential to properly situate each vertebral body, pelvis and femur to accurately study the biomechanical response and injury outcome during UBB loading.

The original lumbar spine FEM was developed based on the CT scan of a post-mortem supine human subject. A literature review [23-30] was conducted to obtain relevant initial orientations for each level of the lumbar vertebral body in a standard 90/90/90 sitting posture (90-degree angle at hip, knee and ankle joints). The orientations between vertebral bodies were defined as the relative angle between mid-vertebral planes of two adjacent vertebral bodies in the lumbar spine (L1-L2, L2-L3, etc.). Based on the available data in literature, the lumbar spine orientation angle for each spine level was selected from a subset of studies which used primarily young healthy human subjects and the average angle is close to the average value of all the studies.

Using the spine orientation angle data (Table 2), the sitting lumbar spine model was constructed by re-orienting the spine angles from those initially modeled. The realignment is completed by rigidly rotating the spine vertebral body in the mid-sagittal plane to the desired orientation angles shown in Table 2. The change in angle between adjacent vertebrae was evenly distributed in the intervertebral discs. This realignment was facilitated using LS-PrePost (LSTC, Livermore, CA USA) scripts without re-mesh.

A side view and comparison of the original versus seated lumbar spine postures is shown in Fig. **3**. A 35 degree pelvic angle was used for the seated posture based on literature data [27, 30]. The femur was rotated to the horizontal plane about the geometric center of the femoroacetabular joint to simulate 90/90/90 seated posture.

Table 2. Segmental angles measured by the angle between the plane of inferior endplate of each vertebral body and horizontal plane for a seated posture.

Spine level	90/90 Sitting
L1	-14.4 ^{o}
L2	-12.8 ^{o}
L3	-5.0 ^{o}
L4	1.1^{o}
L5	13.2 ^{o}

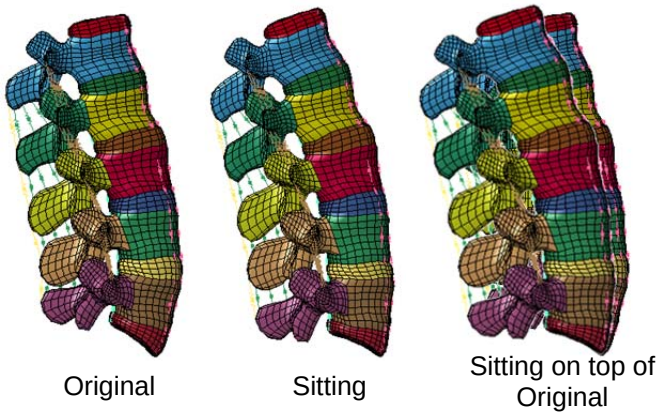

Fig. 3 Comparison of lumbar spine in seated posture with original spine posture from visible human

Loading Conditions

Simulations using full-body Hybrid-III dummy FEM were conducted with low and high vertical seat accelerations to obtain pelvis accelerations for the high-fidelity lumbar/pelvis/femur FEM (Fig. 4) [31, 32]. The whole pelvis acceleration traces including both positive and negative phases were applied to the bottom of the ischial tuberosity of the lumbar/pelvis/femur following SAE-J211 coordinate system.

A mass of 54.1 kg was rigidly attached to the superior surface of T12/L1 intervertebral disc and L1 posterior elements to simulate the inertial loading from torso mass. The mass, moment of inertia and location of the center-of-gravity were obtained from a previously developed human torso model [33]. The point mass was located at (2, 9, 12) mm from the center of the T12/L1 intervertebral disc. An additional 28 kg mass, located 10 cm posterior to the torso CG was used to simulate the torso-borne mass. As shown in Table 3, a total of four loading scenarios were simulated using a combination of low and high pelvis accelerations, with and without the torso-borne mass. Simulations were carried out using a commercial nonlinear dynamic finite element solver LS-DYNA (LSTC, Livermore, CA USA). The explicit formulation LS-DYNA is a widely used and well accepted commercial finite element solver in simulating structural response under blast loading [34, 35].

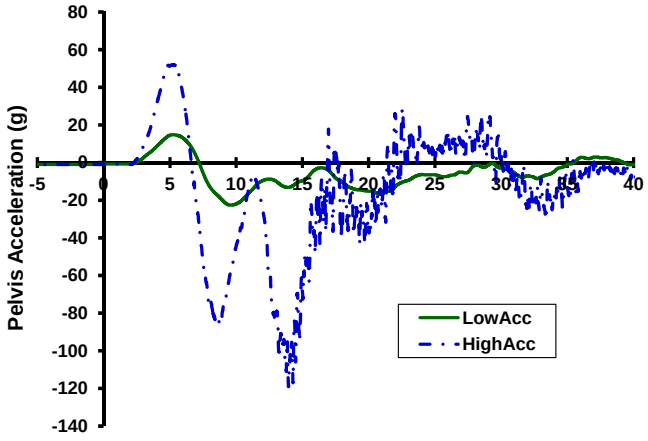

Fig. 4. Pelvis accelerations from Hybrid-III FEM applied to the ischial tuberosity of the high-fidelity lumbar/pelvis/femur model

Table 3. Loading and torso-borne mass conditions

Pelvis acceleration	Without Torso-borne mass	With Torso-borne mass
Low Acc	Case 1	Case 3
High Acc	Case 2	Case 4

The torso displacement and acceleration were obtained from the motion of the rigid torso mass. Relative displacements between adjacent spine levels at anterior and posterior aspects of the mid-sagittal plane (Fig. 5a) were analyzed to study the level specific spine kinematics. Total segmental normal and shear forces, bending moments and torque were analyzed in correlation to lumbar spine injury at the mid-vertebral cross-section of

the vertebral body (Fig. 5b, c) from the high-fidelity lumbar/pelvis/femur FEM.

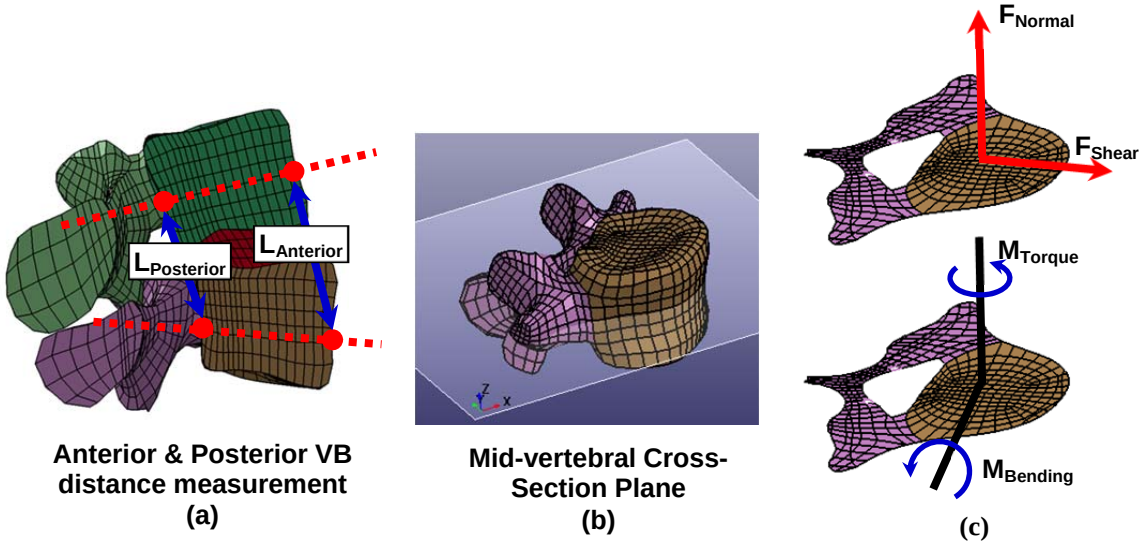

Fig. 5 Illustration of post-process to calculate distance between adjacent level and cross-sectional normal/shear force and bending/torque moment.

III. RESULTS

The finite element simulations were carried out to approximately 40 ms for the simulations with low pelvis acceleration (Case 1 & Case 3), and 20 ms for the simulations with high pelvis acceleration (Case 2 and Case 4). Force, moment and intervertebral disc deformation exceeded injurious levels during the simulation [21, 36].

Displacements and accelerations of the torso mass for Case 1 and Case 2 are shown in Fig. 6. For Case 1, the torso was pushed cranially 10.4 mm and posteriorly 3.1 mm under the pure vertical seat acceleration. Lateral displacement is minimal due to the symmetry of the model. Maximum peak acceleration of 10.5g was found in the Z direction (approximately 1/2 of the pelvis acceleration 21.9g) and 3.7g in the X direction. For Case 2, peak acceleration of 27.8g was found in the Z direction (approximately 1/5 of the seat acceleration 139.2g) and 10.3g in the X direction at approximately 20 ms.

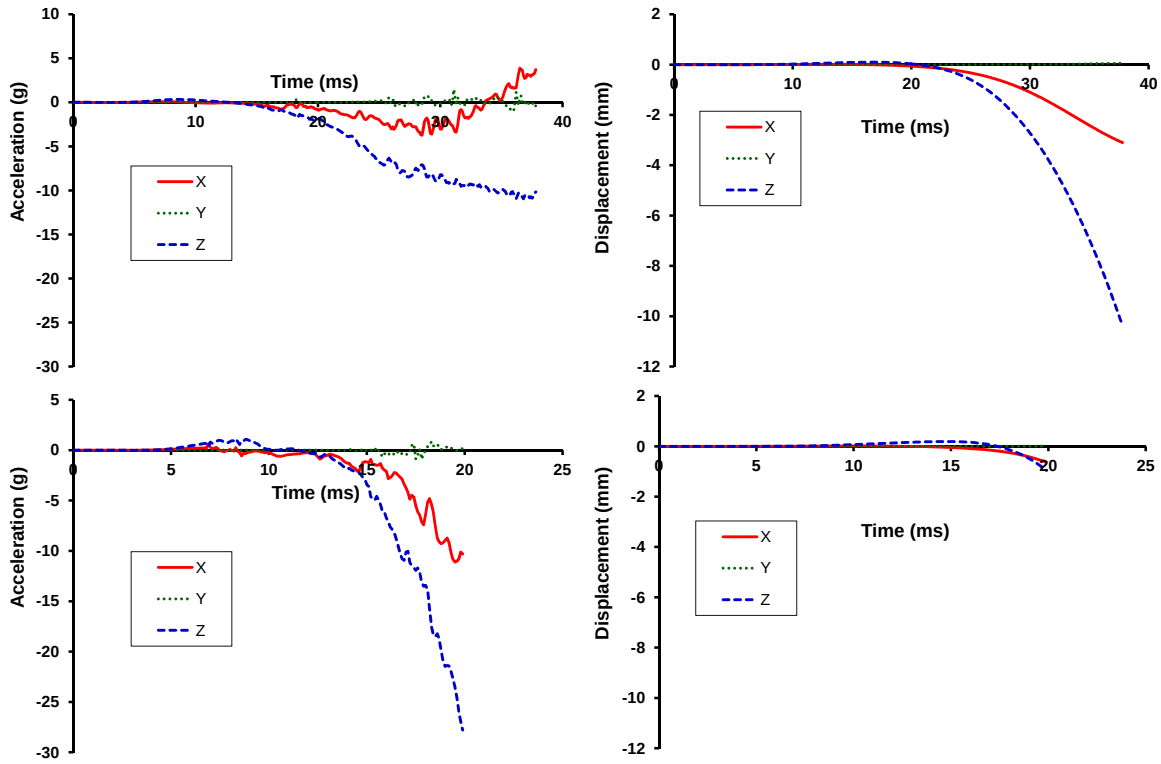

Fig. 6 Torso acceleration and displacement history for Case 1 (top) and Case 2 (bottom)

Relative displacement (Fig. 5a) between L1-L2, L2-L3, L3-L4, L4-L5 at anterior and posterior of the mid-sagittal plane for Case 1 were shown in Fig. 7. Maximum compression was found in L1-L2 anterior (-8.5 mm, at 37.8 ms), whereas maximum distraction was found in L4-L5 (4.9 mm, at 37.8 ms).

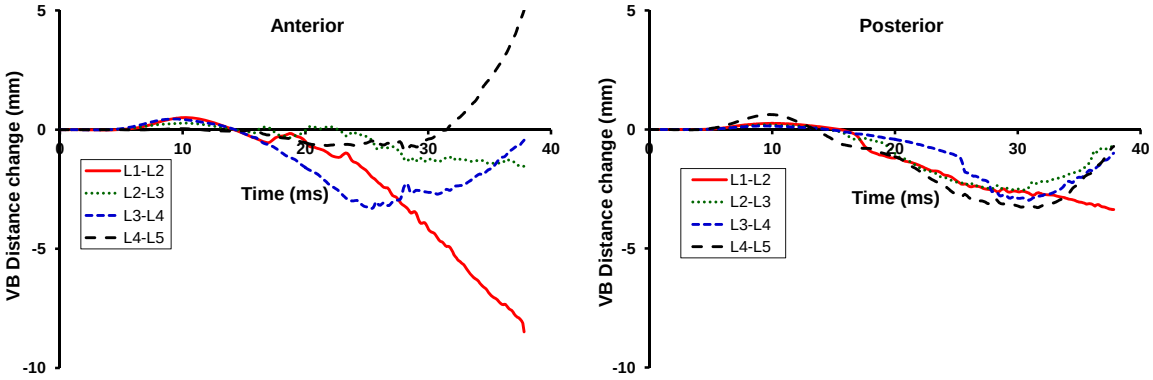

Fig. 7 Distance change between anterior and posterior of vertebral body for Case 1.

Normal, transverse and resultant cross-sectional forces from mid-vertebral plane (Fig. 5b,c) of the vertebral body of L1-L5 for Case 1 are shown in Fig. 8. Similarly, torque, bending and resultant moment (Fig. 5b,c) are shown in Fig. 9.

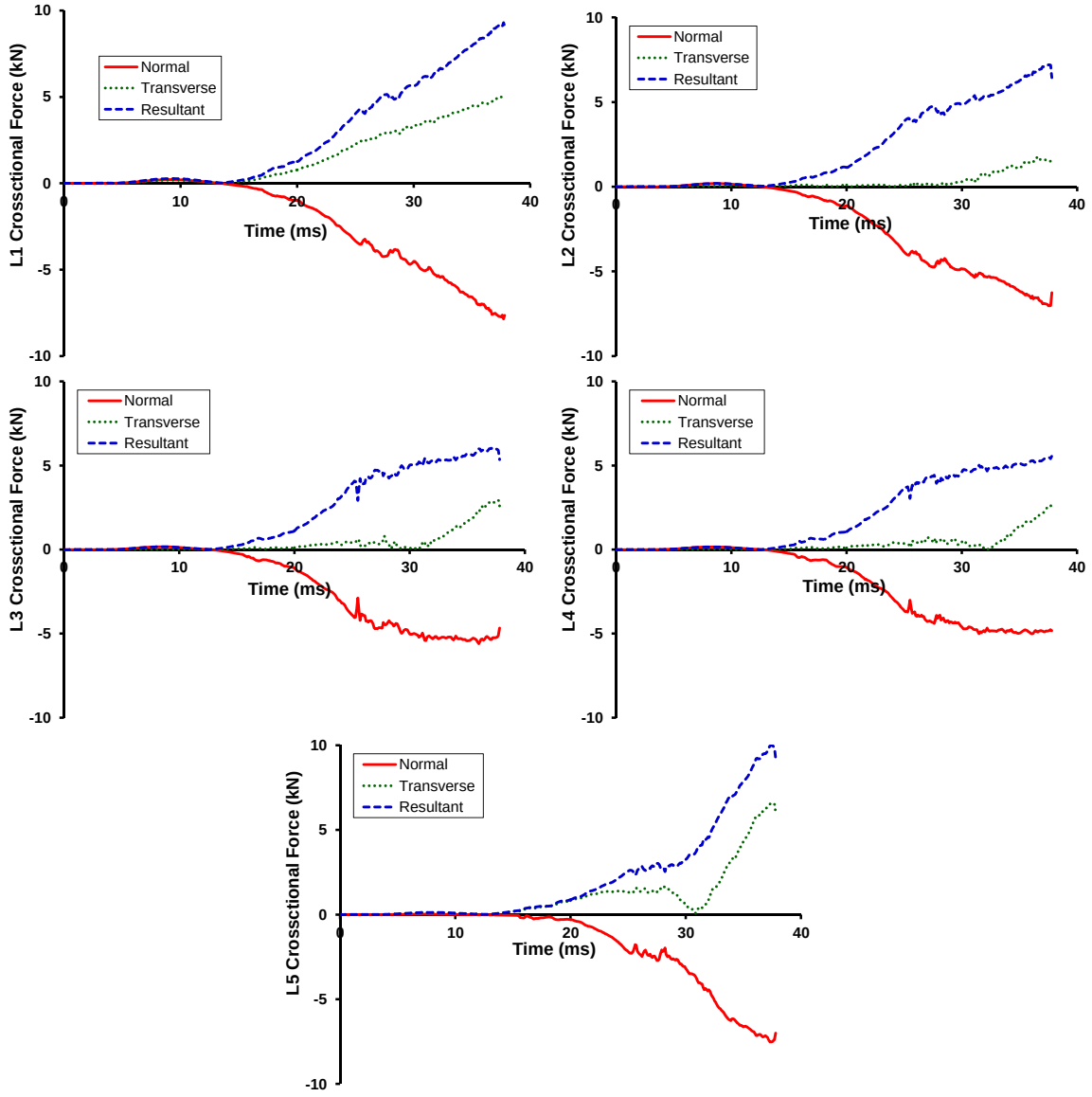

Fig. 8. Normal, transverse and resultant cross-sectional force (Fig. 5b,c) at mid-vertebral plane for L1-L5 for Case

1.

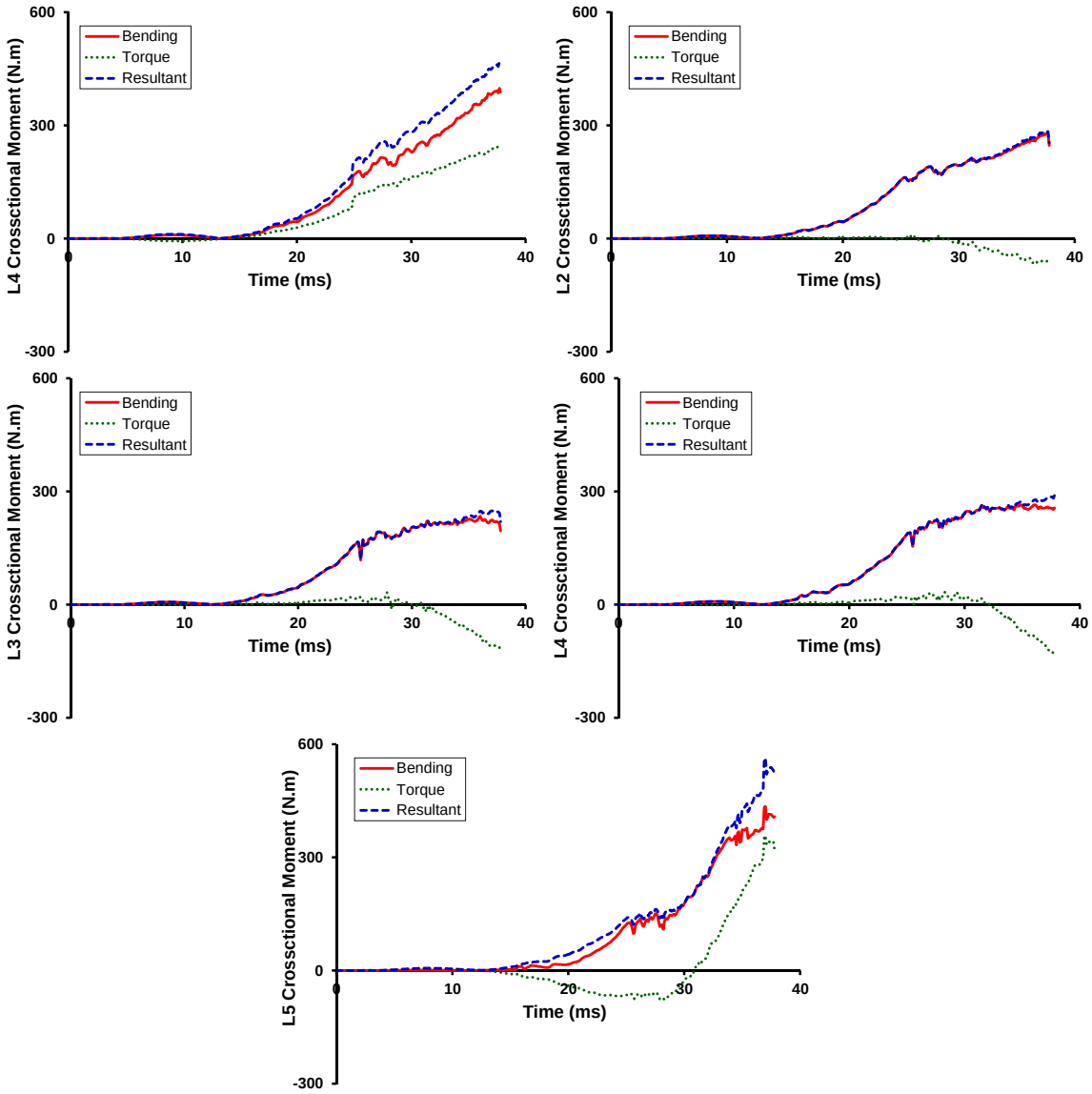

Fig. 9. Torque, bending and resultant cross-sectional moment at mid-vertebral plane (Fig. 5b,c) for L1-L5 for Case 1.

Resultant cross-sectional force and cross-sectional moments were compared between the four loading scenarios in Fig. 10.

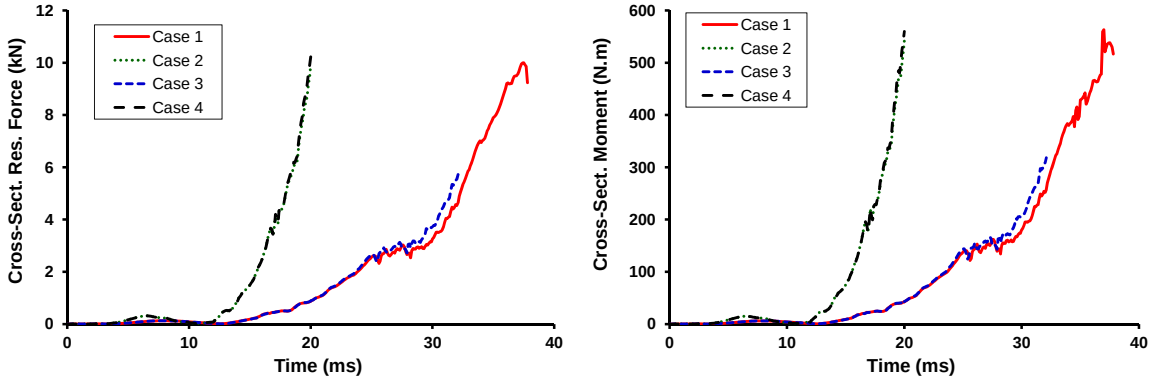

Fig. 10. Comparison of resultant cross-sectional force and moment at mid-vertebral plane (Fig. 5b,c) between 4 loading scenarios.

IV. DISCUSSION

The geometry generalization procedures used in the current study resulted in a generic 50th percentile lumbar spine model without the strong correlation to its initial subject. Detailed quantitative 3-D measurement for the width and depth of upper and lower endplate, and posterior vertebral height from L1 to L5 were compared to results reported by Panjabi et al in Fig. 11 [37].

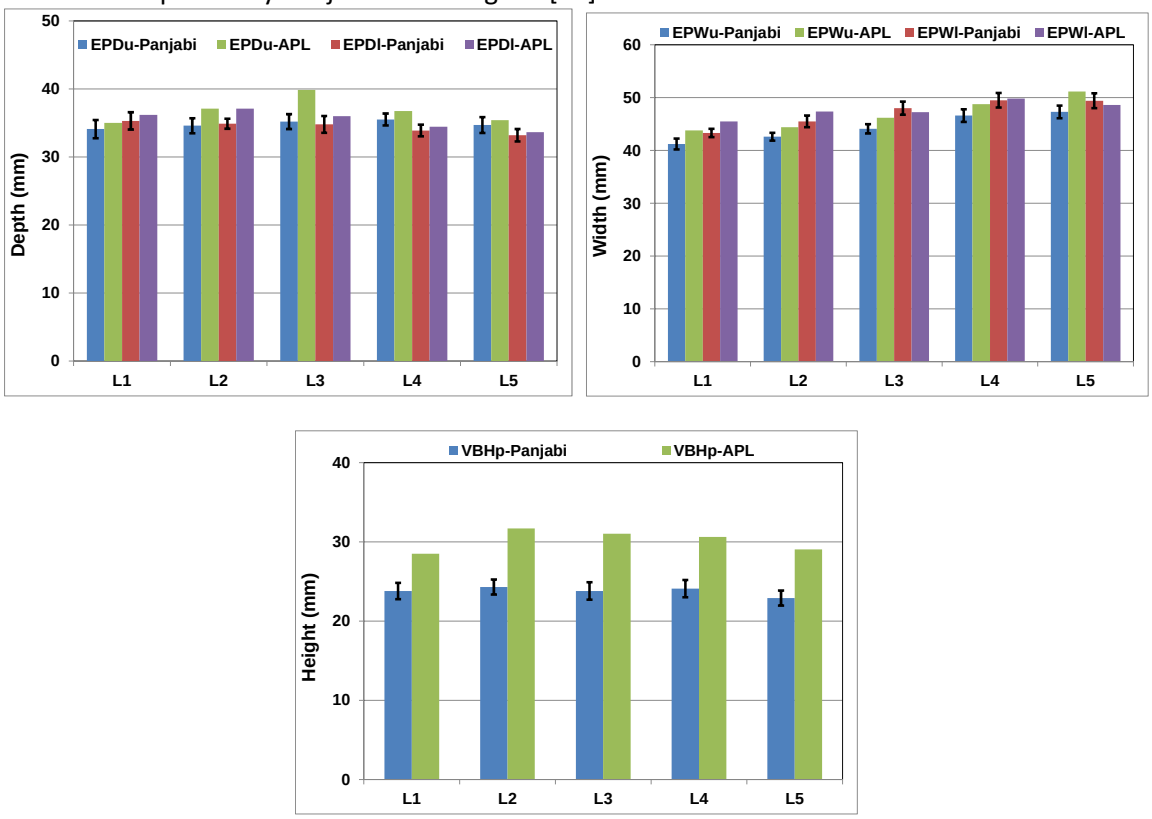

Fig. 11 A detailed comparison spine dimension measurements of the current study to reported literature data [37]. (EPDu: upper endplate depth; EPDl: Lower endplate depth; EPWu: upper endplate width; EPWl: lower endplate width; VBHp: posterior height of vertebral body; -Panjabi: literature data; -APL: measurement of the current model)

Results demonstrated the dimensions of the current model matched closely to literature reported data for the endplate depth and width for upper (EPDu, EPWu) and lower endplate (EPDl, EPWl) of each spine level (L-L5). However, the posterior vertebral body heights (VBHp) were consistently higher compared to literature reported data, with the difference ranged from 4.7-7.4mm and relative difference of 16% to 23%). The reported literature data included both male and female subjects (8/4), with average age of 46.3 (19-59) yrs, and average height of 167.8 (15-178) cm. Whereas, the current model is from a male subject at age 39 yrs and scaled to 50th percentile height (178 cm). The difference in subject gender, age and height may explain the systematically higher vertebral height in the current study. Overall the dimension of the current lumbar spine model matched closely to literature reported data and represented generic 50th percentile male subject lumbar spine geometry.

As direct measurement of UBB loading to PMHS lumbar spine is currently not available in literature, a Hybrid-III whole body FEM was used as an indirect method to obtain lumbar spine loading. The Hybrid-III FEM simulations were conducted with idealized UBB loading. Pelvis acceleration from the Hybrid-III FEM was used as input to the high-fidelity pelvis lumbar spine model. The output from lumbar spine load cell in the Hybrid-III was not used because vertical load transfer through the Hybrid-III was considered as not realistic due to the inherent structural design of the Hybrid-III dummy. Instead, pelvis acceleration was considered as a direct measurement of pelvis to seat contact force that was least affected by the properties of Hybrid-III. The hypothesis is the anatomically accurate pelvis and femur model can provide more realistic load transfer and boundary condition to the lumbar spine than the Hybrid-IIII. Currently the pelvis and femur are both treated as linear elastic material. They were included in the model to provide a more realistic load transfer and boundary condition. The injuries of pelvis and femur during UBB loading may be considered in future studies by including material failure.

In order to accurately study the biomechanical response of the lumbar spine during UBB loading, accelerative loading from the seat needs to be properly transmitted to the spine through the pelvic structure. To achieve this goal, a previously-developed lumbar spine model was extended to include the pelvis and femur geometries to allow vertical pelvic acceleration to be properly modulated through the pelvis structure and the femur mass. Relevant vertical load profiles were obtained from pelvis acceleration predicted by a full-body Hybrid-III dummy model. Each level of the lumbar spine, pelvis and femur were appropriately oriented to the 90/90/90 sitting posture based on literature data.

Three features of our model allow the UBB loading to be properly transmitted through the human skeletal structure for accurate biomechanical response simulation: 1) the use of a Hybrid-III full-body model to transfer seat acceleration to the pelvis; 2) the accurate geometry and proper posture of femur, pelvis and lumbar spine; and, 3) the use of high-rate material models for intervertebral disc annulus and nucleus.

All four simulation cases were terminated before the cross-sectional force and moments reached peak values; however, the time of termination for all the simulations (~40 ms for Case 1, 3 and ~20 ms for Case 2, 4) included the time of peak input pelvis acceleration (~10 ms for low pelvis acceleration, ~15 ms for high pelvis acceleration). In addition, at the time of termination, cross-sectional forces and moments have reached ~10 kN and ~580 N.m respectively (Fig. 10). These values exceed reported ultimate strength of lumbar spine vertebrae in compression (~2.9-8.6 kN) and intervertebral disc in bending (~33 N.m), indicating spine failure is very likely to occur [21, 36, 38-41]. The large force and moments in the lumbar spine also caused severe deformation of the intervertebral disc leading to numerical instabilities beyond the time of termination.

For Case 1, the torso mass had a global displacement ~10.4 mm cranially and 3.1 mm posteriorly at ~40 ms (Fig. 6 top). For Case 2, the global displacement for the torso mass was less than 1 mm (~1 mm cranially and 0.6 mm poseriorly) by the end of 20 ms, although maximum acceleration (27.8g, at 20 ms) was 2.6x larger than Case 1 (10.5g at 40 ms) (Fig. 6). By 20 ms, severe deformation occurred in the elements at the lower parts of lumbar spine. Cross-sectional force and moments have exceeded lumbar spine ultimate strength [21, 36, 38-41].

These results indicate that under severe pelvis acceleration, the lumbar spine will likely fail before the torso mass is affected by the acceleration. The T12/L1 junction is close to a rigid boundary condition without the need to use a simulated torso mass. The motion of the torso mass is not insignificant under low pelvis acceleration. PMHS testing of lumbar spine under lower pelvis acceleration should consider attaching a torso mass to simulate inertial loading from torso and torso-borne mass.

Relative displacement between adjacent spine levels reveals vertebral-body specific loading modes. Relative posterior displacements for all spine levels were reasonably similar, ranging from 2.5mm to 3.3 mm compression at approximately 30 ms. However, relative anterior displacements showed significant difference from level to level. Maximum compression was found between L1-L2 with approximately 8.5 mm compression, at 37.8 ms. The anterior compression was approximately 2.6x larger than the posterior compression, indicating a flexion motion between L1-L2. On the contrary, the anterior aspect of L4-L5 went into distraction after 30 ms with maximum distraction of 4.9 mm at 37.8 ms. The posterior compression was approximately 1mm at this time. The anterior distraction and posterior compression indicated a relative extension mode between L4-L5. The flexion (bending forward) in the upper level and extension (bending backward) in the lower level of the lumbar spine ultimately leads to an “S” shape deformation pattern in the lumbar spine.

Analysis of cross-sectional force and moment (Fig. 5b,c) provides insight into the loading mode at each spine level. Although the model is left/right symmetric and the pelvis acceleration is purely vertical, measureable torque moment was observed across L1-L5 (Fig. 9). This is because the torso model that was used to calculate the torso mass was not left/right symmetric. This resulted in a CG location 9 mm off form the mid-sagittal plane. This off center torso CG mass resulted into lateral bending and coupled axial motions which lead to the observed measureable torque along the spine. A comparison of resultant force and moments for Case 1 showed relatively small difference from level to level. However, the distribution between normal and transverse force (Fig. 8), torque and bending moment (Fig. 9) has significant variation between levels. To quantify the change of distribution, the ratio of peak transverse to peak normal force and peak torque to peak bending moment for Case 1 was calculated (Fig. 13).

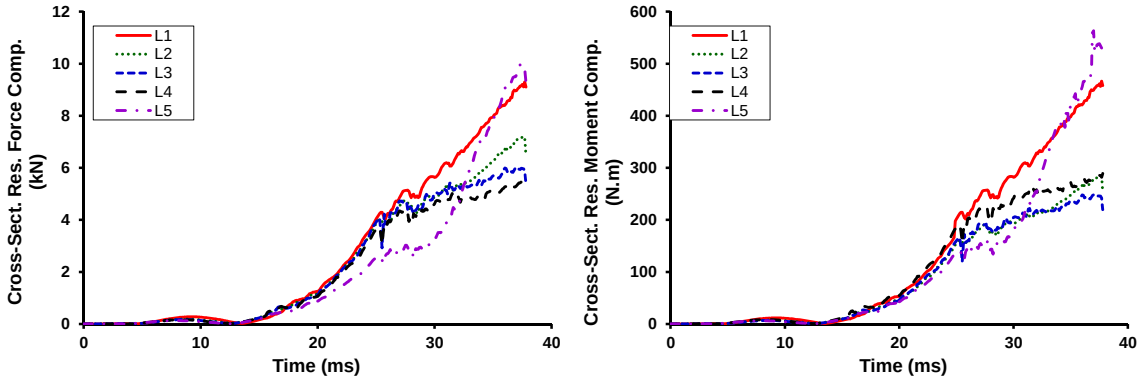

Fig. 12. Comparison of resultant cross-sectional force and moment at each spine level for Case 1.

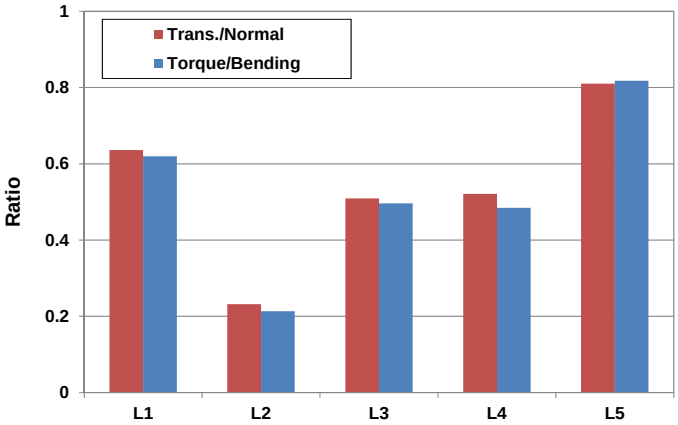

Fig. 13 Ratio of transverse to normal force and torque to bending moment at each spine level for Case 1.

As shown in Fig. 13, none of the calculated transverse to normal or torque to bending moment ratios exceed a value of 1.0, indicating the UBB loading induced a primarily compressive and bending loading to the spine. The small transverse to normal force ratio (~0.2) at L2 level indicated a major compressive loading with relative small percent of shear at this level. Transverse shear to normal force ratio ranged from 0.5-0.6 at L1, L3, L4 and was approximately 0.8 at L5. The significantly larger shear and torque loading components at these levels indicated a more complex loading mode at these spine levels.

From the analysis of relative distance change between adjacent spine levels and the distribution of normal to shear force, bending to torque moment, it is evident that the loading mode changes progressively from combined compression/flexion at higher levels, to primarily compression in the mid-level and distraction at lower levels. The progressive change of loading mode from higher level to lower level may also indicate possible change of fracture types along the lumbar spine during UBB loading. Flexion moment combined with compression loading can induce wedge and Chance fractures; compression injuries, such as burst fractures, can occur under major compression loading; while extension moment can lead to distraction injuries [42].

Comparing load cases with and without torso-borne mass (Case 1 vs. Case 3 and Case 2 vs. Case 4), the addition of 28 kg torso-borne mass (approximately 52% of torso mass) only led to a maximum of 20% increase in cross sectional force and moments Fig. 10 for the simulated duration. One potential explanation is that the deformation of the lumbar spine largely absorbed the accelerations from the pelvis, which leads to lesser inertia effects from the torso-borne mass. Since the cross-sectional force and moments have exceeded lumbar spine failure loading, it can be concluded that under the loading severity used in the current study, the torso-borne mass did not have a determining effect on the early response of lumbar spine before lumbar spine injury occurred [21, 36, 38-41].

However, it should be indicated that the severity of pelvis accelerations are relatively high and the simulations were terminated at early stage (20 ms and 40 ms) in part due to the severe deformation of elements in the intervertebral disc. As demonstrated in the study, the effects of inertial loading from torso and torso-borne mass cannot be ignored under lower severities of pelvis acceleration. In addition, the difference in cross-sectional force and moment between with/without torso-borne mass may increase at a later stage of

spine response. Therefore, the effects of torso-borne mass may have a much large effect at a later stage of the spine deformation under lower pelvis accelerations than those used in the current study.

V. LIMITATION

Limitations of the current study include the use of finite element modeling method. As with all finite element model studies, the reported results are linked to geometry, material model, boundary, initial and loading conditions used in the current study.

Efforts to generalize the model geometry, including scale to 50th percentile and force left/right symmetry, have been taken to ensure the model geometry represents a larger population instead of tied to a particular human subject used for the study.

Validation of model was completed under major loading model of vertical UBB loading, i.e., axial compression in the sagittal plane, ensuring the model response from material properties used in the current study matches well to literature quasi-static experimental data. However, it should be pointed out, due to the paucity of experimental data at UBB loading, the current model has only been validated to quasi-static loading. JHU APL is currently in the process of producing high-rate dynamic loading experimental data. The current model will be continuously validated and improved as new experimental data been generated to better simulate the response of high-rate dynamic loading interested in UBB loading scenario.

Initial posture of the lumbar spine may also have significant impact on the model response and possible injury outcome. The current model has prescribed a posture representing generic 90/90/90 sitting posture based on reported literature data. The 90/90/90 posture has been considered as a starting point for lumbar spine biomechanical response study during UBB loading. However, it should be pointed out that the lumbar spine sitting posture were based on literature for subjects without body-borne weight. Literature has shown additional body-borne weight will change lumbar spine posture. The change of spine posture due to additional weight bearing was not considered in the current study.

Respond from a finite element model is also linked to the boundary and loading conditions. The current model used pure vertical pelvis loading obtained from a Hybrid-III simulation under generic UBB loading. A non-fracture pelvic model was included to provide a better boundary condition and force transfer to the lumbar spine. Only two loading severity were considered. As loading severity and directions change, or if pelvis fractures before the lumbar spine, response from the model will also change. The effects of loading direction, other loading severities beyond current study, and effect of pelvis fracture on lumbar spine injury maybe considered in future studies.

VI. CONCLUSIONS

The current study extends a previously developed lumbar spine model to include pelvis and femur structures. The pelvis and spine posture was adjusted for more accurate load transfer from seat acceleration to the lumbar spine during UBB loading.

The global motion of the torso mass cannot be ignored under low pelvis accelerations. However, the severe pelvis acceleration was large enough to cause lumbar spine failure regardless of additional torso mass. Analysis of relative distance changes between lumbar spine levels and the cross sectional force and moment found a progressively changing loading mode from higher levels to lower levels with flexion between L1-L2, and extension between L4-L5, and primarily compression in the mid-level. The change of loading model and an “S” shape deformation indicated possible change of fracture mechanisms along the spine under the UBB loading. The torso-borne mass has limited impact on early lumbar spine response during the time duration (20-30 ms) investigated in the current study. For the loading severity investigated in the current study, lumbar spine injury will occur before the torso-borne mass will be fully engaged. The effect of torso-borne mass may increase at later stages of the UBB loading with lower severity of pelvis acceleration.

These results may provide biomechanical insight to explain mechanisms of lumbar spine injuries observed during UBB events, and guide the design of injury mitigation devices to reduce field injury.

VII. ACKNOWLEDGEMENT

This effort was funded by contract # W81XWH-09-2-0168. The U.S. Army Medical Research Acquisition Activity, 820 Chandler Street, Fort Detrick MD 21702-5014 is the awarding and administering acquisition office. The content included in this work does not necessarily reflect the position or policy of the U.S. government.

VIII. REFERENCES

1. Gondusky, JS and MP Reiter, Protecting military convoys in Iraq: an examination of battle injuries sustained by a mechanized battalion during Operation Iraqi Freedom II, *Mil Med*, 170(6):546-9, 2005.
2. Alvarez, CJ, Epidemiology of Blast Injuries in Current Operations, in RTO-MP-HFM-207 - A Survey of Blast Injury across the Full Landscape of Military ScienceNATO: Halifax, CANADA. p. KN1-10,2011.
3. Ragel, BT, et al., Fractures of the thoracolumbar spine sustained by soldiers in vehicles attacked by improvised explosive devices, *Spine*, 34(22):2400-5, 2009.
4. Schoenfeld, AJ, GP Goodman, and PJ Belmont, Jr., Characterization of combat-related spinal injuries sustained by a US Army Brigade Combat Team during Operation Iraqi Freedom, *Spine J*, 12(9):771-6, 2012.
5. Ramasamy, A, et al., Blast mines: physics, injury mechanisms and vehicle protection, *J R Army Med Corps*, 155(4):258-64, 2009.
6. Kargus, RG, et al., Methodology For Establishing The Mine/IEd Resistance Capacity Of Vehicle Seats, *Army Research Laboratory*Adelphi, MD 20783-1197, 2008.
7. Scherer, R, C Felczak, and S Halstead. Vehicle and Crash Dummy Response to an Underbelly Blast Event; Available from: https://blastinjuryresearch.amedd.army.mil/docs/ubb/Vehicle_and_Crash_Dummy_response_to_an_underbelly_blast_event.pdf,2011.
8. Galbusera, F, et al., The effect of degenerative morphological changes of the intervertebral disc on the lumbar spine biomechanics: a poroelastic finite element investigation, *Comput Methods Biomech Biomed Engin*, 14(8):729-39, 2011.
9. Schmidt, H, et al., Response analysis of the lumbar spine during regular daily activities--a finite element analysis, *Journal of Biomechanics*, 43(10):1849-56, 2010.
10. Schmidt, H, et al., Effect of multilevel lumbar disc arthroplasty on spine kinematics and facet joint loads in flexion and extension: a finite element analysis, *Eur Spine J*, 2010.
11. Rohlmann, A, et al., Effect of a pedicle-screw-based motion preservation system on lumbar spine biomechanics: a probabilistic finite element study with subsequent sensitivity analysis, *Journal of Biomechanics*, 43(15):2963-9, 2010.
12. Kraft, RH and SL Wozniak, A Review of Computational Spinal Injury Biomechanics Research and Recommendations for Future Efforts, *Army Research Laboratory*,ARL-TR-5673, 2011.
13. Ruan, J, et al., Prediction and analysis of human thoracic impact responses and injuries in cadaver impacts using a full human body finite element model, *Stapp Car Crash J*, 47:299-321, 2003.
14. Ruan, JS, et al., Impact response and biomechanical analysis of the knee-thigh-hip complex in frontal impacts with a full human body finite element model, *Stapp Car Crash J*, 52:505-26, 2008.
15. Zhang, J, et al., A High-Fidelity Model for Lumbar Spine Injury Investigation during Under Body Blast Loading, in RTO-MP-HFM-207 - A Survey of Blast Injury across the Full Landscape of Military ScienceNATO: Halifax, CANADA. p. 1-12,2011.
16. Ackerman, MJ, The Visible Human Project: a resource for anatomical visualization, *Stud Health Technol Inform*, 52 Pt 2:1030-2, 1998.
17. Segars, WP, et al., 4D XCAT phantom for multimodality imaging research, *Med Phys*, 37(9):4902-15, 2010.
18. Slavin, KV, The Visible Human Project, *Surg Neurol*, 48(6):638-9, 1997.
19. Iwaskiw, AS, et al., Response of individual thoracolumbar spine ligaments under high-rate deformation, *Biomed Sci Instrum*, 48:194-201, 2012.
20. Ott, KA, et al., Method for obtaining simple shear material properties of the intervertebral disc under high strain rates, *Biomed Sci Instrum*, 48:324-31, 2012.
21. Dooley, CJ, et al., Response of Thoracolumbar Vertebral Bodies to High Rate Compressive Loading, *Biomed Sci Instrum*, 49:In Press, 2013.
22. Shirazi-Adl, A and M Parnianpour, Nonlinear response analysis of the human ligamentous lumbar spine in compression. On mechanisms affecting the postural stability, *Spine (Phila Pa 1976)*, 18(1):147-58, 1993.
23. Bridger, RS, C Von Eisenhart-Rothe, and M Henneberg, Effects of seat slope and hip flexion on spinal angles in sitting, *Hum Factors*, 31(6):679-88, 1989.
24. De Carvalho, DE, et al., Lumbar spine and pelvic posture between standing and sitting: a radiologic investigation including reliability and repeatability of the lumbar lordosis measure, *J Manipulative*

Physiol Ther, 33(1):48-55, 2010.
25. Dunk, NM, et al., Evidence of a pelvis-driven flexion pattern: are the joints of the lower lumbar spine fully flexed in seated postures?, *Clin Biomech (Bristol, Avon)*, 24(2):164-8, 2009.
26. Ferrari, R, Sitting biomechanics, Part II: optimal car driver's seat and optimal driver's spinal model, *J Manipulative Physiol Ther*, 24(2):140-3, 2001.
27. Harrison, DD, et al., Sitting biomechanics part I: review of the literature, *J Manipulative Physiol Ther*, 22(9):594-609, 1999.
28. Lee, YH and YL Chen, Regressionally determined vertebral inclination angles of the lumbar spine in static lifts, *Clin Biomech (Bristol, Avon)*, 15(9):672-7, 2000.
29. Troyanovich, SJ, et al., Radiographic mensuration characteristics of the sagittal lumbar spine from a normal population with a method to synthesize prior studies of lordosis, *J Spinal Disord*, 10(5):380-6, 1997.
30. Yasukouchi, A and T Isayama, The relationships between lumbar curves, pelvic tilt and joint mobilities in different sitting postures in young adult males, *Appl Human Sci*, 14(1):15-21, 1995.
31. Mohan, P, et al., LSTC / NCAC Dummy Model Development, in 11th International LS-DYNA Users Conference: Detroit, MI, USA. p. 53-64,2010.
32. Arepally, S, et al., Application of Mathematical Modeling in Potentially Survivable Blast Threats in Military Vehicles, *US Army RDECOM-TARDEC*Warren, MI, USA, 2008.
33. Roberts, JC, et al., Computational and experimental models of the human torso for non-penetrating ballistic impact, *J Biomech*, 40(1):125-36, 2007.
34. William, K and F Fillion-Gourdeau, Numerical simulation of light armoured vehicle occupant vulnerability to anti-vehicle mine blast, in 7th International LS-DYNA Users Conference: Dearborn, MI, USA. p. 7-14,2002.
35. Williams, K, et al., Validation of a loading model for simulating blast mine effects on armoured vehicles, in 7th International LS-DYNA Users Conference: Dearborn, MI, USA. p. 35-44,2002.
36. Neumann, P, et al., The ultimate flexural strength of the lumbar spine and vertebral bone mineral content, *J Spinal Disord*, 6(4):314-23, 1993.
37. Panjabi, MM, et al., Human lumbar vertebrae. Quantitative three-dimensional anatomy, *Spine (Phila Pa 1976)*, 17(3):299-306, 1992.
38. Adams, MA, et al., Posture and the compressive strength of the lumbar spine, *Clin Biomech (Bristol, Avon)*, 9(1):5-14, 1994.
39. Adams, MA, TPF Green, and P Dolan, The Strength in Anterior Bending of Lumbar Intervertebral Discs, *Spine*, 19(19), 1994.
40. Osvalder, AL, et al., Ultimate strength of the lumbar spine in flexion--an in vitro study, *J Biomech*, 23(5):453-60, 1990.
41. Skrzypiec, DM, et al., Shear strength of the human lumbar spine, *Clin Biomech (Bristol, Avon)*, 27(7):646-51, 2012.
42. Magerl, F, et al., A comprehensive classification of thoracic and lumbar injuries, *Eur Spine J*, 3(4):184-201, 1994.